Climate Dynamics (2003) 20: 301–313
DOI 10.1007/s00382-002-0271-7

H. Renssen · P.W. Bogaart

Atmospheric variability over the ~14.7 kyr BP stadial-interstadial transition in the North Atlantic region as simulated by an AGCM

Received: 7 December 2001 / Accepted: 14 June 2002 / Published online: 5 September 2002

Abstract The ECHAM4-T42 atmospheric general circulation model was applied to study the change in atmospheric variability in the North Atlantic region over the ~14.7 kyr cal BP climatic transition from Greenland Stadial 2a (GS-2a, end of Pleniglacial) to Greenland Interstadial 1e (GI-1e, start Late Glacial). The following three climates are simulated: (1) present-day, (2) GS-2a and (3) GI-1e. We focus on climatic parameters near the Earth's surface (temperature, precipitation and sea level pressure). Results on two different temporal scales are analysed: seasonal and daily. The seasonal fields show that the main change over the 14.7 kyr BP transition occurred in winter. We calculated daily standard deviations of temperature and pressure about the seasonal means and the high-pass filtered (less than six days) variability of pressure. The largest change in atmospheric variability occurred in northwest Europe. Here, the daily temperature variability decreased by 50%, whereas storm activity also decreased substantially. These changes are related to a northward shift of the Atlantic sea-ice margin at 14.7 kyr BP, leading to a northward relocation of the Atlantic storm track. In the GS-2a experiment, a strong storm track was located over northwest Europe, where frequent depressions produced alternations of northerly air flow (below –30 °C) and southerly air flow (close to 0 °C). This strong daily atmospheric variability decreased in GI-1e because the storm track had a SW-NE orientation over the Atlantic towards Iceland. The decrease in atmospheric variability at 14.7 kyr BP probably contributed to landscape stabilization, for instance, through decreasing eolian transport.

H. Renssen (✉) · P.W. Bogaart
Netherlands Centre for Geo-ecological Research (ICG),
Faculty of Earth and Life Sciences,
Vrije Universiteit Amsterdam, De Boelelaan 1085,
NL-1081 HV Amsterdam, The Netherlands
E-mail: renh@geo.vu.nl

H. Renssen
Institut d'Astronomie et de Géophysique
Georges Lemaître, Université Catholique de Louvain,
2 Chemin du Cyclotron, B-1348 Louvain-la-Neuve,
Belgium

1 Introduction

Numerous proxy data show that the last glacial climate in the North Atlantic region was characterized by rapid climatic shifts between cold stadial conditions and relatively warm interstadial conditions (e.g. Johnsen et al. 1992; Bond et al. 1993). A well-documented example of these shifts is the transition from Greenland Stadial 2a (GS-2a, or Late Pleniglacial) to Greenland Interstadial 1e (GI-1e or 'Bølling') that occurred at ~14.7 kyr cal BP (calendar years before present, see. Björck et al. 1998). Isotopic evidence from the GISP2 ice core indicates that during this transition mean annual temperatures over Greenland increased by 9 °C within a few decades (Severinghaus and Brook 1999). Comparable temperature changes have been reconstructed for the North Atlantic Ocean surface (e.g. Bard et al. 1987; Koç and Jansen 1994) and terrestrial sites in Europe (e.g. Atkinson et al. 1987; Lowe et al. 2001; Renssen and Isarin 2001). Experiments with coupled atmosphere-ocean climate models strongly suggest that the stadial-interstadial transitions were caused by changes in the strength of the thermohaline circulation in the North Atlantic Ocean (Sakai and Peltier 1997; Ganopolski and Rahmstorf 2001). Further study of these climatic transitions and their impact on the environment is highly desirable, as this provides important information on the response of the geo-system during phases of rapid climate change.

Recently, Renssen and Isarin (2001) studied the change in mean seasonal temperatures over the 14.7 kyr BP stadial-interstadial transition in Europe by comparing atmospheric general circulation model (AGCM) results with reconstructions based on multi-proxy data. The model results were in good agreement

with the paleodata. Renssen and Isarin (2001) concluded that the major temperature increase at 14.7 kyr BP was mainly a winter signal, with values increasing by more than 15 °C over northern Germany (from –21 °C to –6 °C) and even 25 °C over Ireland (from –25 °C to 0 °C). During summer the warming over the continent was less spectacular with a temperature rise of 3 to 6 °C at 55°N. It was suggested that the main factor controlling the strong increase in temperatures was the position of the winter sea-ice edge in the North Atlantic Ocean. In the AGCM experiments it was assumed that during GS-2a winters the Atlantic Ocean was ice-covered down to ~48°N, whereas for GI-1e an ice-free central North Atlantic was prescribed with a sea-ice margin following the line Greenland-Iceland-Scotland.

In addition to shifts in temperature, stadial-interstadial transitions were also characterized by changes in atmospheric circulation. This is clearly evidenced by fluctuations in the content of dust and wind-transported chemical elements in Greenland ice cores (Mayewski et al. 1994). The atmospheric circulation of cold glacial phases is the subject of many climate model studies (e.g. Rind 1987; Joussaume 1993; Valdes and Hall 1994; Renssen et al. 1996; Hostetler et al. 1999; Kageyama et al. 1999a, b; Kageyama and Valdes 2000). In these studies the differences with present-day conditions are considered. The climate model studies show that the increased meridional gradient in glacial climates produced an intensified extra-tropical atmospheric circulation when compared to today, with stronger jet streams and extended mid-latitude storm tracks that are displaced eastward and follow a more zonal path (e.g. Kageyama et al. 1999a). However, these differences with the present interglacial conditions do not necessarily reflect changes occurring over stadial-interstadial (cold-cool) transitions. After all, *interstadial* climates were very different from the modern state, due to a number of factors such as the presence of extensive icesheets in North America and Europe, cooler oceans and a sparse vegetation cover. Because of these environmental conditions, it is likely that interstadial climates, as exemplified by the Lateglacial Bølling-Allerød period, are intermediate between the stadial and present (i.e. interglacial) climate states.

Knowledge of changes in daily atmospheric variability over stadial-interstadial transitions is important, as they strongly influenced environmental processes. For instance, a change in the frequency and magnitude of storms could have an important impact on eolian processes (e.g. Vandenberghe 1991; Kasse 1997) and river activity (e.g. Huisink 1997). The aim of this study is, therefore, to analyze the change in daily variability over the 14.7 kyr BP stadial-interstadial transition in the North Atlantic region, utilizing AGCM experiments on GS-2a and GI-1e performed with the ECHAM4 atmospheric general circulation model. The same experiments were used by Renssen and Isarin (2001) to estimate the GS-2a-GI-1e temperature change in Europe. We explore the spatial patterns of daily variability by plotting maps of daily standard variations in temperature and sea level pressure, and by investigating the changes in storm tracks. Moreover, we look in detail at a local scale by analyzing the average daily result of five grid-cells centred around ~52°N, 6°E. Our results are useful for better understanding of climate system evolution during the last glacial, for the interpretation of paleoenvironmental records (e.g. Bohncke 1993; Hoek 1997; Vandenberghe and Nugteren 2001) and for modeling studies on sedimentological processes during the Late Quaternary (e.g. Leeder et al. 1998; Bogaart and van Balen 2000; Veldkamp and Tebbens 2001).

2 Model and experimental design

2.1 Model

We analyze results of three experiments performed with the ECHAM4-T42 (European Centre/HAMburg) AGCM of the Max Planck Institute for Meteorology, Hamburg. This global model has nineteen atmospheric levels and a horizontal resolution of ~2.8 degrees latitude-longitude (i.e. T42 version). ECHAM4 includes both annual and diurnal cycles, and simulates the global atmospheric circulation, including directly related climatic variables as temperature, wind strength and direction, precipitation and evaporation. A detailed description of ECHAM4 is found in DKRZ (1994) and Roeckner et al. (1996). ECHAM4-T42 is designed to simulate climate at a sub-continental to global scale and it simulates a modern climate that corresponds reasonably with observations (Roeckner et al. 1996). Moreover, the ECHAM model includes a satisfactory representation of mid-latitude storm-tracks (Kageyama et al. 1999a).

2.2 Experiments

In three equilibrium experiments we aimed to simulate the climates of today (control experiment, hereafter named CTRL), GI-1e (hereafter expGI1e) and GS-2a (hereafter expGS2a). They represent three different types of climates: interglacial (CTRL), interstadial (expGI1e) and stadial (expGS2a). CTRL is a reference simulation with present-day boundary conditions prescribed, such as surface ocean conditions, topography, land–sea-ice distribution, land surface characteristics, insolation and atmospheric concentrations of greenhouse gases (Table 1). To simulate the climates of GS-2a and GI-1e, these modern boundary conditions were altered in expGS2a and expGI1e in accordance with the geological and paleoecological records from these periods. The changes in boundary conditions are described in detail by Renssen and Isarin (2001), so here only a brief overview is given.

2.2.1 Surface ocean conditions

In expGS2a and expGI1e we altered the ocean surface conditions prescribed in CTRL, which are based on the 1979–1988 mean that was compiled from various sources by Reynolds (1988). As no global data sets of sea surface temperatures (SSTs) are available for GS-2a and GI-1e, we had to make assumptions on the basis of available paleoceanographic data. The prescribed SSTs in expGS2a and expGI1e should therefore be considered as approximations of the surface ocean conditions during GS-2a and GI-1e. In expGS2a we prescribed the global set of glacial sea surface temperatures and sea-ice conditions published by CLIMAP members (1981). In the Atlantic Ocean, this implies sea-ice margins at 48°N and 60–65°N for winter and summer seasons, respectively. South of the sea-ice margins, the prescribed SST anomaly decreased with latitude, from up to 10 °C cooler than CTRL near Europe to a cooling of less

Table 1 Design of three experiments analyzed in this study. The duration of the experiments (in model years) is indicated next to the experimental names. The prescribed atmospheric CO_2 concentrations of are given in ppmv, whereas the concentrations of CH_4 and N_2O are expressed in ppbv. In this table, 'k' denotes cal kyr BP. See text for further information

	CTRL (16 yr) Modern	ExpGI1e (12 yr) 'Bølling'	ExpGS2a (12 yr) 'Late Pleniglacial'
SSTs + sea-ice	0 k	Nordic seas covered by sea-ice	Global (CLIMAP)
Ice sheets	0 k	14 k	15 k
Insolation	0 k	14.5 k	15 k
$CO_2/CH_4/N_2O$	353/1720/310	220/650/220	220/450/220
Vegetation parameters	0 k	'Bølling'	Glacial

than 2 °C in the tropics (Renssen and Isarin 2001). In the Pacific Ocean, we removed the pools with SSTs warmer than today, as we considered these unlikely, although it should be noted that glacial SSTs are still under debate (e.g. Crowley 1994, 2000; Guilderson et al. 1994; Mix et al. 2001). In expGI1e we prescribed a sea-ice cover that followed the line Greenland-Iceland-Scotland in winter (i.e. ice-covered Nordic Seas), whereas during summer we placed the sea-ice margin at 65–66°N (i.e. latitude of Iceland). We assumed that GI-1e SSTs in the central North Atlantic Ocean (i.e. south of 60°N) were comparable to today, implying a strong thermal gradient from 60°N northwards (Renssen and Isarin 2001). These surface ocean conditions for GI-1e are in general agreement with proxy data for the North Atlantic Ocean (e.g. Koç et al. 1993, 1996).

2.2.2 Other boundary conditions

In expGS2a and expGI1e, the following boundary conditions were also changed compared to CTRL: topography, vegetation parameters, insolation and concentration of greenhouse gases (see Table 1 and Renssen and Isarin 2001). The topography was changed in expGS2a and expGI1e according to Peltier (1994). The most important changes were the addition of extensive Laurentide and Scandinavian icesheets. The prescribed maximum elevations for the Laurentide icesheet were about 2.1 km (expGS2a) and 1.5 km (expGI1e), whereas these values for the Scandinavian Icesheet were about 1.5 km (expGS2a) and 1.2 km (expGI1e). A further modification was the conversion of the land–sea mask to account for a lower sea level, with the change from sea to land in the North Sea region as the most important adjustment. Moreover, to take vegetation changes into account, we altered the following land surface parameters: surface background albedo, surface roughness, leaf area index, vegetation cover and forest cover. We based the latter changes on the global vegetation reconstructions of Adams and Faure (1997), and on the set of land surface parameters published by Claussen et al. (1994). Furthermore, insolation was changed according to Berger (1978) and atmospheric concentrations of greenhouse gases were altered in agreement with measurements in Antarctic ice cores (e.g. Raynaud et al. 1993; Flückiger et al. 1999).

3 Simulated atmospheric variability

Our objective is to present results that may be useful for the interpretation of geological and paleoecological records and therefore, we focus on climatic parameters near the Earth's surface (2 m temperatures, sea level pressure and precipitation). Results on two temporal scales are analyzed: seasonal means (December–January–February versus June–July–August) and daily means.

3.1 Seasonal means

Seasonal results are plotted as expGI1e–expGS2a anomalies to show the simulated changes occurring over the 14.7 kyr BP transition. The mean DJF changes are plotted in Fig. 1a–d and reflect mainly the effect of prescribed differences in North Atlantic Ocean surface conditions. The disappearance of the extensive sea-ice cover in expGI1e leads to much higher air temperatures (i.e. maximum of 40 °C difference) over the North Atlantic and its sea boards than in expGS2a (Fig. 1a). Moreover, the main precipitation belt changes from a zonal path in expGS2a, mainly between 45 and 50°N, to one with a more meridional SW–NE axis in expGI1e. As a result, the expGI1e–expGS2a precipitation anomaly (Fig. 1b) shows a decrease over the western North Atlantic between 45 and 50°N, whereas an increase is noted over the rest of the North Atlantic region. This general increase is related to the warmer air in expGI1e (increasing the vapour holding capacity) and the northward shift in sea-ice cover in expGI1e (making a moisture source available). The modelled sea level pressure (SLP) (Fig. 1c, d) reveals a change from relatively high pressure in expGS2a, due to subsidence over the partial sea-ice cover and cold ocean waters, to a clearly expressed Icelandic Low in expGI1e. However, in expGS2a the pressure minimum is located closer to the European coast, creating a steeper pressure gradient over northwest Europe.

In summer the differences between expGI1e and expGS2a are smaller than in winter (see also Renssen and Isarin 2001). In the JJA temperature plot, the maximum warming of more than 10 °C is located at 45°N (Fig. 2a). More to the North the temperature rise becomes smaller (i.e. 6 to 8 °C), following the CLIMAP (1981) SST reconstruction. The simulated expGI1e–expGS2a anomalies for precipitation have the same pattern as in DJF, although less pronounced (Fig. 2b). The SLP plots reveal relatively little change, as the north–south pressure gradients during JJA are similar in both simulations (Figs. 2c, d).

3.2 Daily variability

Changes in daily variability are explored in two ways. First, the spatial pattern of daily variability is studied by plotting maps of the daily standard deviation about the seasonal mean for temperature and SLP. Also the high-pass filter of Hoskins et al. (1989), which singles out perturbations on a time-scale or less than six days, is applied to SLP data to find the changes in storm tracks during the winter season. This filter has also been used

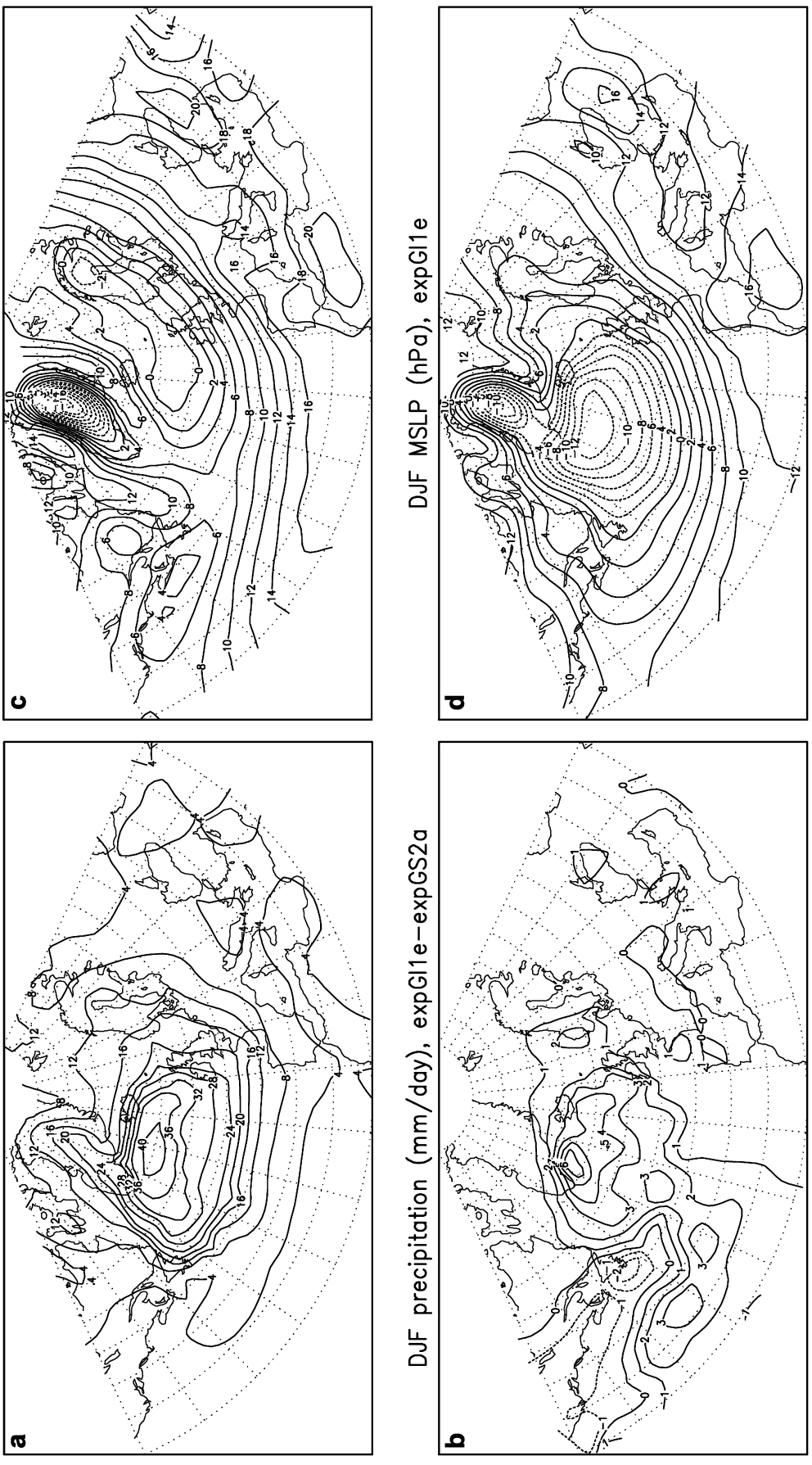

Fig. 1 Simulated mean DJF change over the 14.7 kyr BP transition: **a** 2 m air temperature (°C) expGI1e–expGS2a anomaly, **b** precipitation (mm/day) expGI1e–expGS2a anomaly, **c** SLP (hPa) in expGS2a, **d** SLP (hPa) in expGI1e. Note that the SLP fields are plotted as anomalies from the global seasonal SLP values to account for pressure differences between experiments due to the introductions of ice-sheets

by Kageyama et al. (1999a) to study atmospheric variability in simulations performed within the Paleo Model Intercomparison Project (PMIP). Second, the evolution of temporal variability is studied by looking at daily mean results for 5 grid cells in northwest Europe (i.e. around 52°N, 6°E, approximately the location of The Netherlands). These grid cells were chosen because it is located at a latitude that is sensitive to climate changes around ~14.7 kyr BP (Coope et al. 1998; Renssen and Isarin 2001). Moreover, it enables us to compare our results with earlier model studies on past climatic changes in The Netherlands (e.g. Isarin et al. 1997; Renssen 2001). Renssen (2001) showed that modern results from the grid cell at 52°N, 5°E compare well with observations, indicating that the model also captures the present-day climatic characteristics at this 'local' scale.

3.2.1 Daily standard deviations about the seasonal mean

In CTRL, the daily temperature standard deviation about the DJF mean varies between 2 and 4 °C in W Europe (Fig. 3a) and clearly increases in a northeastern direction (i.e. to more continental conditions) to 8–10 °C in Finland and NW Russia. Over the Atlantic Ocean the daily standard deviation is mostly below 2 °C. Modern observations suggest higher values (between 2 and 5 °C) over the northern North Atlantic (e.g. Tucker and Barry 1984). It is likely that the lower standard deviations in CTRL can be partly attributed to the prescription of SSTs. In expGI1e and expGS2a, the picture looks very different compared to CTRL, as the maximum DJF values are found over North Atlantic Ocean near the prescribed winter sea-ice margins (Fig. 3b, c). The daily DJF standard deviation in expGS2a is highest between 50 and 55°N (more than 14 °C), with a tongue of high standard deviation values (between 10–14 °C) spreading eastward over Northwest Europe. Relatively low values (6–8 °C) are also found over the Scandinavian Icesheet. In JJA, daily standard deviations are in the range of 2 to 4 °C, with values slightly increasing when the climate becomes colder (not shown).

Daily SLP standard deviations about the DJF mean show a maximum along the sea-ice edge in the Atlantic Ocean. In CTRL, this maximum is over 15 hPa and is located over the Nordic Seas between Svalbard and Norway. (Fig. 4a). This result agrees well with observations for the present climate, except north of 55°N, where these data suggest a higher maximum (over 18 hPa) that is located near Iceland (e.g. Tucker and Barry 1984). In expGI1e and expGS2a, the highest DJF SLP standard deviation is more to the south, reflecting the different prescribed sea-ice conditions (Fig. 4b, c). In contrast, in JJA all three experiments have produced similar results, with maximum daily JJA SLP deviations of more than 8 hPa over the Atlantic Ocean west of Scotland (not shown). This pattern is very similar to what is found in modern observations (Tucker and Barry 1984).

3.2.2 Storm tracks

The high-pass filtered standard deviations give insight into SLP variability that is associated with depression activity (i.e. storm tracks). In Fig. 5a it is shown that the centre (over 7 hPa) of the DJF storm activity for CTRL follows a path from Newfoundland to the Nordic Seas between Iceland and the Norwegian coast. Data for the modern climate suggest that the model simulates the position of the storm track correctly, but slightly underestimates the maximum activity (over 9 hPa instead of 7 hPa, see e.g. Kageyama et al. 1999a). In the result for expGI1e (Fig. 5b), the core of the storm track has moved eastward compared to CTRL. The storm track in expGI1e has a similar SW-NE orientation as in CTRL, but a higher variability (more than 8 hPa) and an extension onto the European continent along 55°N (see 7-hPa isobar). In expGS2a, the picture is very different (Fig. 5c), with much higher values (maximum over 11 hPa) and a more zonal orientation that implies high storm activity over much of northwest Europe (values between 8 and 10 hPa). The latter result looks very similar to the storm tracks computed by Kageyama et al. (1999a) for LGM experiments performed with ECHAM3 (i.e. a previous version of the same model). This correspondence is expected, as we prescribed in expGS2a the same ocean surface conditions (i.e. CLIMAP 1981) and comparable other boundary conditions. It should be noted that in LGM simulations with other AGCMs, the Atlantic storm track is less strong than indicated by the ECHAM model (Kageyama et al. 1999a). Although our results indicate that the storm activity decreases over the GS-2a–GI-1e transition, in Europe the amount of precipitation increases at the same time (Fig. 1b). This is related to the prevailing rule that warm air is more humid than cooler air (i.e. has a greater vapour holding capacity) and to the disappearance of the sea-ice cover over the North Atlantic in GI-1e, making available an important moisture source for precipitation (Kageyama et al. 1999a; Renssen and Isarin 2001).

3.3 Discussion

In summary, when considering the European continent, our results show that over the GS-2a–GI-1e transition the largest changes in atmospheric variability occurred during winter in northwest Europe (Britain, Ireland, northern France and the Low Countries). Here, the daily temperature standard deviation about the DJF mean suggests a decrease in the day-to-day temperature variability of at least 50% going from GS-2a to GI-1e (compare Fig. 3b, c). Moreover, the high frequency SLP variability indicates a strong decrease in storm activity in this region (compare Fig. 5b, c). Of course, this noted change is strongly associated with the changes in North Atlantic surface conditions that we prescribed in our experiments. The main difference between expGS2a and

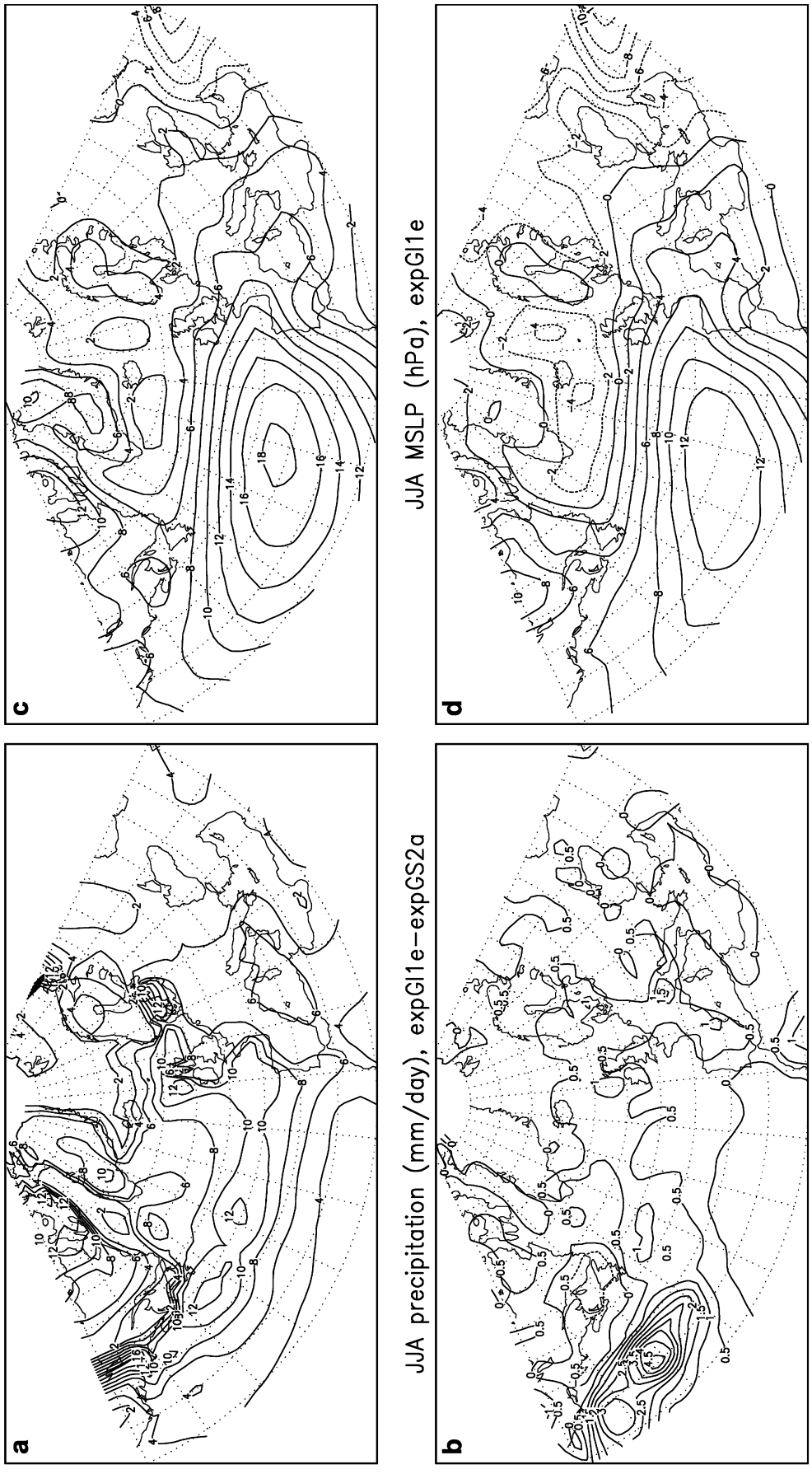

Fig. 2 Simulated mean JJA change over the 14.7 kyr BP transition (difference between expGI1e and expGS2a): **a** 2 m air temperature (°C) expGI1e–expGS2a anomaly, **b** precipitation (mm/day) expGI1e–expGS2a anomaly, **c** SLP (hPa) in expGS2a, **d** SLP (hPa) in expGI1e

expGI1e is the ice-cover over the central North Atlantic Ocean (down to 48°N). In expGS2a, the air is strongly cooled over this sea-ice cover (below –30 °C), whereas to the south the prescribed SSTs force the air temperatures to be relatively high (between 0 and +4 °C). The resulting steep thermal gradient produces a larger baroclinic instability near the sea-ice edge, causing mixing of the polar and temperate air masses, and a maximum in daily temperature variability. Moreover, a relatively vigorous atmospheric winter circulation has developed. Thus, in expGS2a, the extended sea-ice cover extends right down to the latitude of mid-latitude storms (45–50°N) and functions as a reservoir of cold air that is transported to northwest Europe when northwesterly to northerly air flow is present there. In contrast, in expGI1e, the winter sea-ice cover was located much more to the north, leading to a storm track with a SW–NE orientation. In northwest Europe, storm activity was less and smaller temperature fluctuations occurred. Moreover, the temperature in northwest Europe remains in expGI1e relatively high due to the proximity of the relatively warm central North Atlantic (forced by prescribed SSTs). However, compared to CTRL, the temperature in northwest Europe is low in expGI1e, mainly because of the Scandinavian icesheet and the cold conditions over the North Sea area. The latter conditions are related to the prescription of land in the southern North Sea, to account for a lower sea level, and winter sea-ice cover in the northern North Sea and Nordic Seas in expGI1e.

Our simulations suggest that outside northwest Europe the changes in variability over the GS-2a–GI-1e

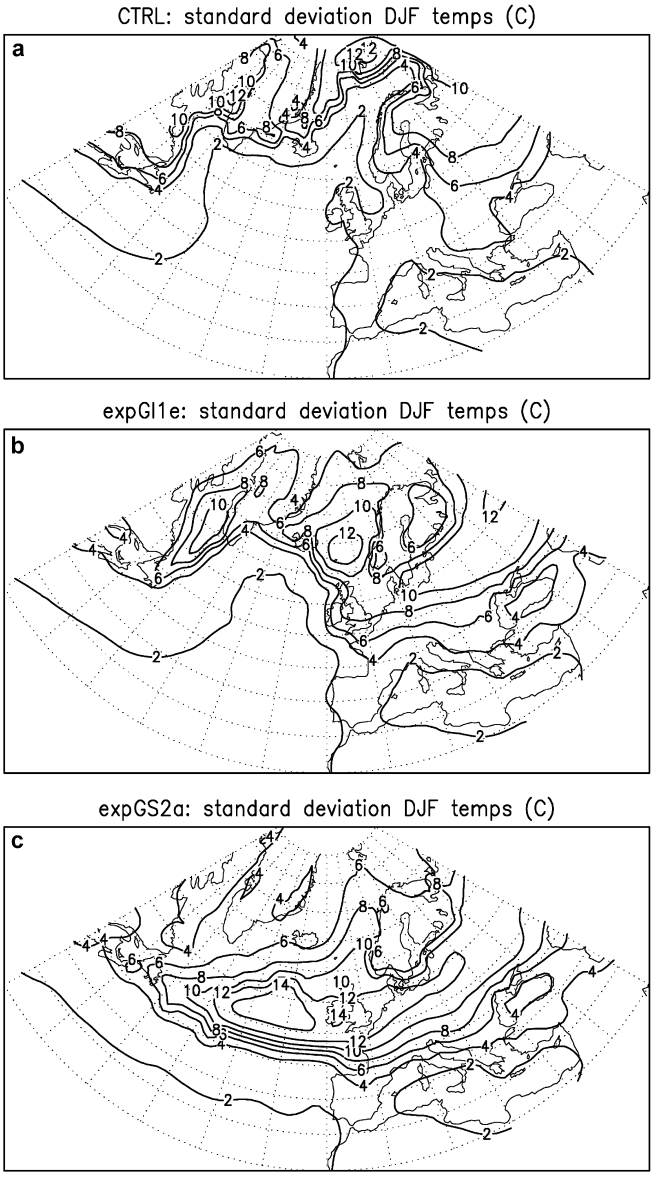

Fig. 3 Daily temperature standard deviation about the DJF mean (°C): **a** CTRL, **b** expGI1e, **c** expGS2a

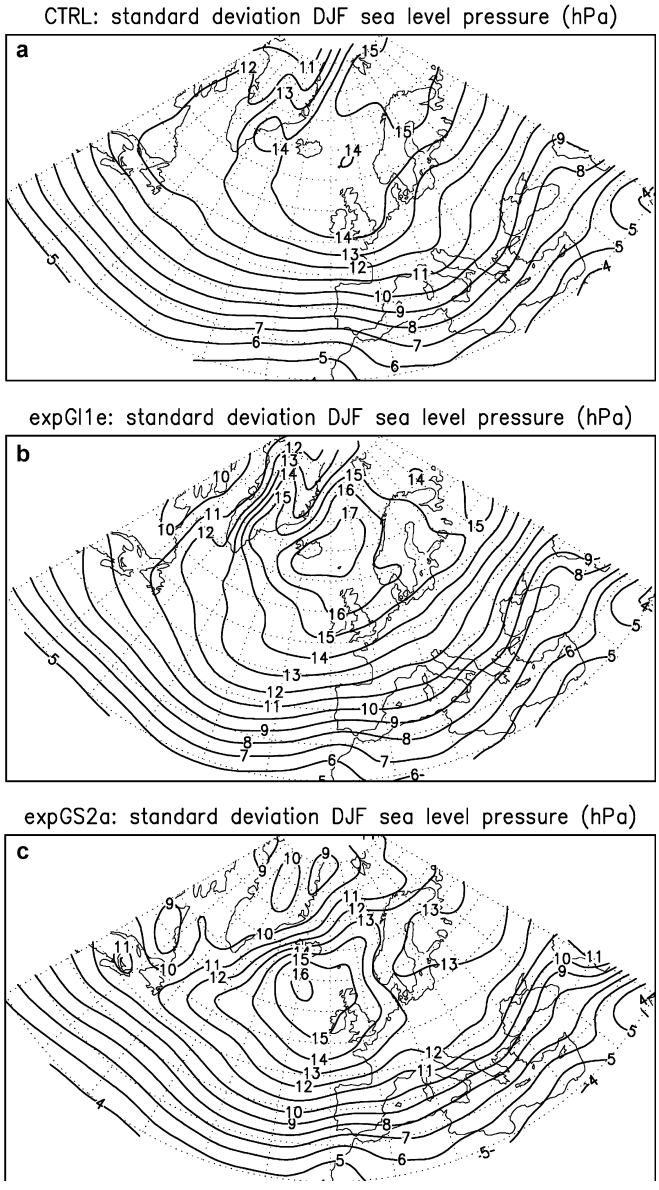

Fig. 4 Daily SLP standard deviation about the DJF mean (hPa): **a** CTRL, **b** expGI1e, **c** expGS2a

transition were relatively small. In southern and eastern Europe, away from the direct influence of the shift in sea-ice cover, the daily atmospheric variability was similar in expGS2a and expGI1e. In the north of our study area, the changes in the prescribed lower boundary conditions were small, as we assumed that the Nordic Seas remained sea-ice covered over the 14.7 kyr BP transition. In addition, the prescribed Scandinavian icesheet was comparable in expGS2a and expGI1e. It is therefore not surprising that we see no significant changes in atmospheric variability over Northern Europe.

Having demonstrated that the largest changes over the 14.7 kyr BP transition occurred in northwest Europe, it is worthwhile to illustrate the effect of the discussed daily atmospheric variability on the model result on a grid-cell scale in this region. In Fig. 6a–c the mean daily temperatures, derived from CTRL, expGI1e and expGS2a, are plotted for a region within the area with maximum variability in northwest Europe (average of five gridcells with the centre at 52°N, 6°E). As expected, the variability is not very different during the summer period (May-August) in the three experiments. During winter, however, the daily temperature variability is much larger in expGI1e and expGS2a than in CTRL. In CTRL, the temperature during DJF is mostly between 0 and 5 °C, with a few cold outbreaks to subzero temperatures of a few days (Fig. 6a). In contrast, in expGI1e the daily temperatures show regular, sharp variations of 15–20 °C around the mean (Fig. 6b), whereas in expGS2a these recurrent temperature shifts are even in the order of 25–35 °C (Fig. 6c). Moreover, in expGS2a the temperature variations are of much shorter duration that in the other experiments. In a simulation on the Younger Dryas climate, the winter temperature variations in this same region were intermediate between expGS2a and expGI1e (Renssen 2001).

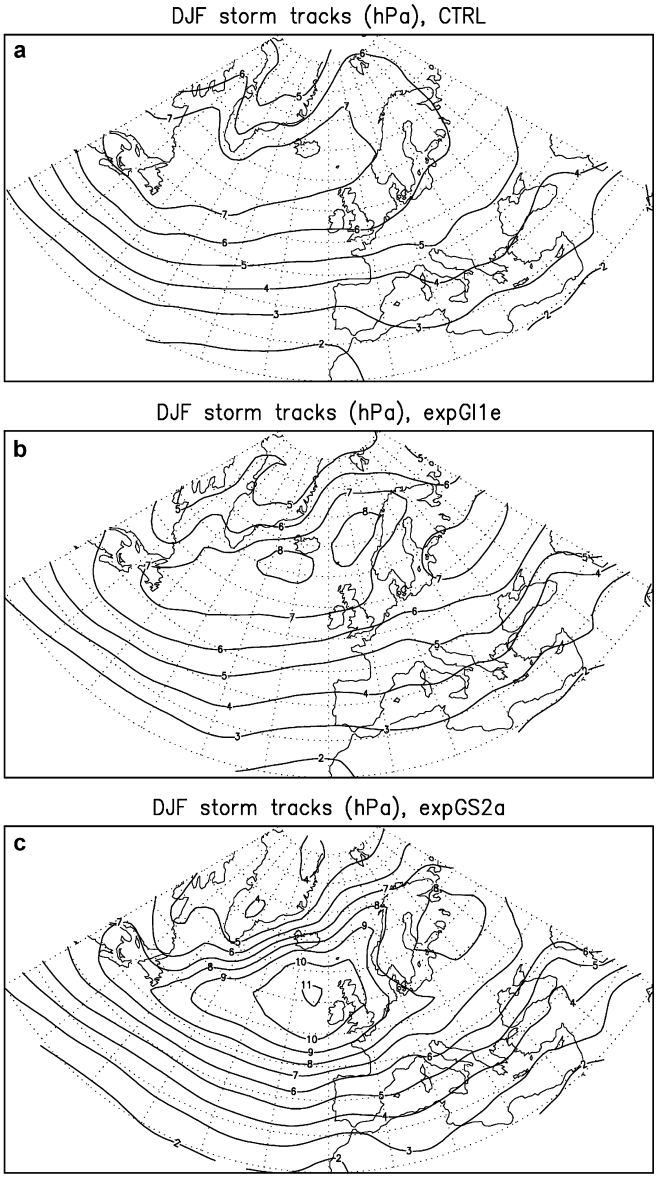

Fig. 5 High-pass (less than 6 days) filtered standard deviation of DJF SLP (hPa): **a** CTRL, **b** expGI1e, **c** expGS2a

The relation between the temperature shifts, SLP variability and North Atlantic surface conditions is further illustrated in Fig. 7. In this figure, the temperature and SLP fields are plotted for four consecutive days around a particular shift in expGS2a (marked in Fig. 6c), starting with relatively cold conditions. This sequence clearly shows that the temperature fluctuations are related to the passage of Atlantic depressions over northwest Europe. A depression moves in four days from 25°W to 30°E from the Atlantic Ocean south of Iceland to Scandinavia (i.e. along 60°N). The warm front associated with this depression, transports relatively warm maritime air with southwesterly winds to northwest Europe, increasing the temperature from less than –40 °C on day 1 to between –5 °C and –10 °C on day 3. After the passage of the depression, the warm anomaly is removed by northerly flow on day 4.

It should be noted that the discussed changes in atmospheric variability over the 14.7 kyr BP transition depend to a large extent on the prescribed surface conditions in the North Atlantic Ocean. The change in atmospheric variability would have been much smaller if a less extensive winter sea-ice cover was prescribed in expGS2a. The latter surface ocean conditions are the subject of an ongoing debate (e.g. Mix et al. 2001). Reconstructions for the LGM based on dinoflagellates suggest an almost ice-free North Atlantic during winter (DeVernal et al. 2000), whereas SST estimates based on foraminiferal modern analogs point to much colder sea-surface conditions with a more extensive sea-ice cover (e.g. Sarnthein et al. 2000). An ice-free North Atlantic during cold glacial phases is however incompatible with terrestrial data that clearly show the presence of permafrost in northwest Europe (Renssen and Vandenberghe 2002), suggesting that the prescribed sea surface conditions in expGS2a may be a reasonable estimate of the state of the North Atlantic during GS-2a.

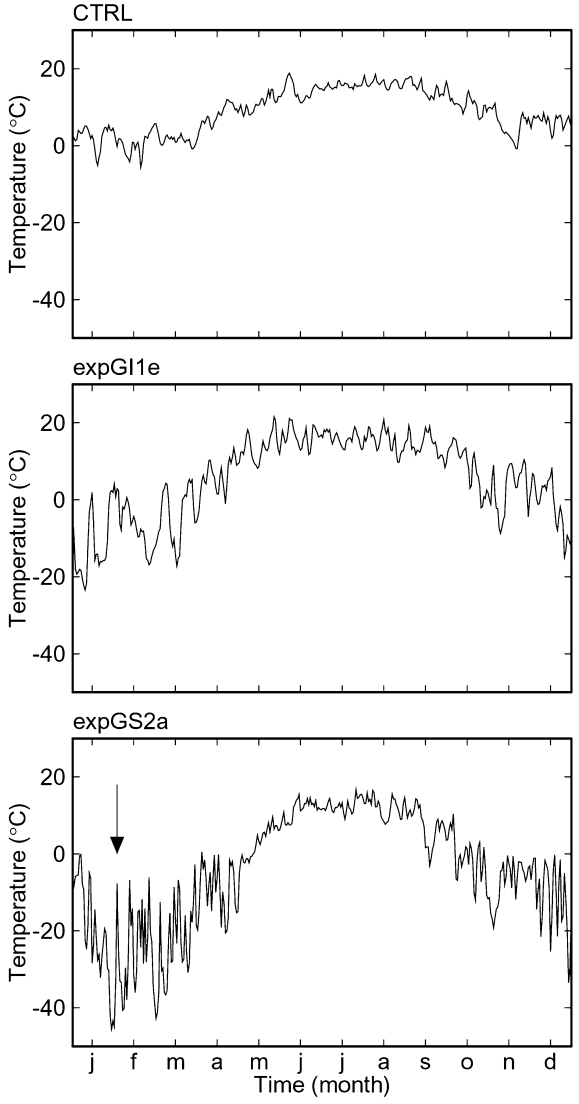

Fig. 6 Mean daily temperatures (°C) for year 3 averaged over five grid cells centred around 52°N, 6°E: **a** CTRL, **b** expGI1e, **c** expGS2a. The *arrow* in **c** signifies the temperature shift analyzed in Fig. 7

4 Potential impact on land-surface processes

It is likely that the inferred sudden decrease in atmospheric variability over the 14.7 kyr BP transition in northwest Europe affected hydrological, geomorphological, sedimentological, ecological and other Earth surface processes. As a detailed investigation of this impact is beyond our scope we only illustrate this point by making a tentative, theoretical analysis of the effects on eolian sediment transport and fluvial activity. Emphasis is on the results obtained from 5 grid cells around 52°N, 6°E.

4.1 Eolian sediment transport

Eolian sediment transport is the main mechanism responsible for the Pleistocene coversand landscape of the Netherlands and other regions in northwest Europe. For the typical grain size of coversands (150–210 μm), saltation begins at a wind speed of 5 m s^{-1} (measured at 10 m, Bagnold 1973). We used the simulated daily wind speed time series (averaged over the five grid cells around 52°N, 6°E), to calculate potential sediment transport fluxes, applying widely accepted equations (Bagnold 1941; Lettau and Lettau 1977):

$$q = 4.2\sqrt{\frac{D}{D_{ref}}}\frac{\rho}{g}u_*^2(u_* - u_{*c})$$

where q is sediment flux [kg m^{-1} s^{-1}], D is median sediment grain size [m], D_{ref} is reference median sediment grain size (0.25 mm) [m], ρ_a is air density [kg m^{-3}], g is gravity [m s^{-2}], u^* is shear velocity [m s^{-1}], u^*_c is threshold shear velocity [m s^{-1}]

Shear velocity u^* is calculated by solving for the near-surface velocity profile:

$$\bar{U}_y = \frac{u_*}{k}\ln\left(\frac{y}{y_0}\right)$$

where $\bar{U}_y$ is time-average velocity at height y [m] (here taken at 10 m), k is von Karman's constant (0.4) and y_0 the roughness length, taken here as y_0 = 0.25 mm, which is appropriate for desert conditions (Allen 1997).

Critical shear velocity u^*_c is calculated from Allen (1997)

$$u_{*c} = A\sqrt{\frac{\rho_s - \rho_a}{\rho_a}gD}$$

where ρ_s is the sediment grain density [kg m^{-3}] and $A \approx 0.1$.

Using these equations, we found 33% more potential eolian sand transport for expGS2a compared to expGI1e. The difference of 33% is mainly attributable to storms during winter (DJF) and spring (MAM) with a mean daily wind speed between 10 and 20 m s^{-1}. No significant difference in the 5–10 m s^{-1} range was found between expGS2a and expGI1e. The CTRL experiment yields similar results as expGI1e. It should be stressed that these equations are only valid for unconfined sand grains on a flat surface. Consequently, this value of 33% represents only the *potential* contribution of a change in wind speed on eolian sand transport, and important factors as differences in vegetation and soil moisture are not taken into account. For instance, it can be argued that actual aeolian transport is hindered by either a frozen soil (permafrost during coldest phases of GS-2), or high moisture content (GI-1e). Nevertheless, Kasse (1997) concludes that, despite these several limiting factors, the entrainment of individual sand grains still occurs due to processes like abrasion, sublimation of soil ice, and evaporation. In summary, the change in storm intensity from GS-2a to GI-1e probably contributed (together with other factors) to the decline in eolian activity within NE-Europe over the GS-2a-GI-1e transition, as reconstructed from sedimentological evidence (e.g. Vandenberghe 1991; Kasse 1997; Bateman and van Huissteden 1999; van Huissteden et al. 2001).

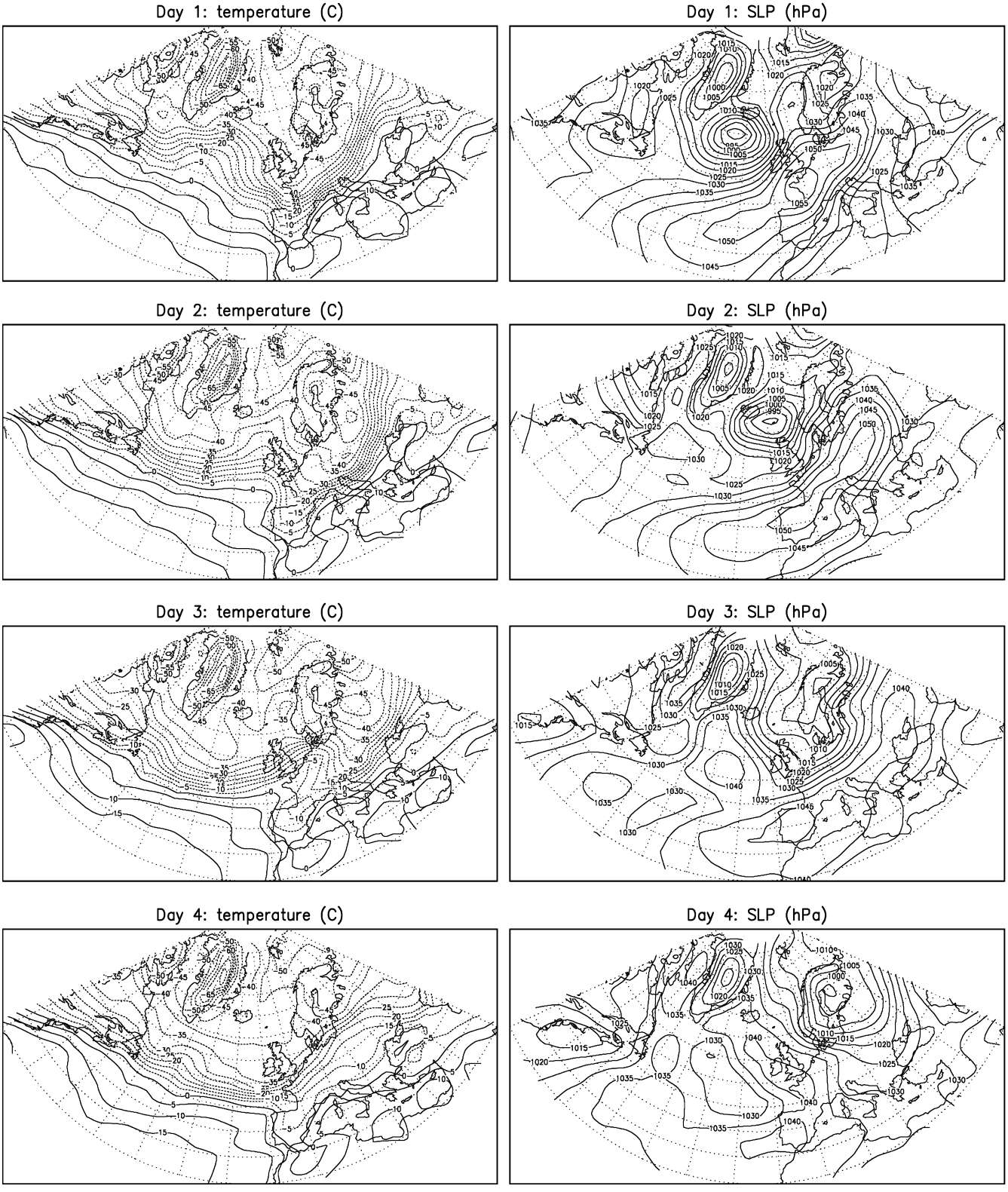

Fig. 7 ExpGS2a: temperature (°C) and SLP (hPa) fields for four consecutive days around temperature shift indicated in Fig. 6c

4.2 Fluvial activity

The impact of the discussed high-frequency atmospheric variability on the dynamics of fluvial systems is likely to be the result of the superposition of a number of processes. For instance, fluvial dynamics are highly sensitive for the frequency and magnitude of water input. Especially in periglacial climates (such as GS-2a), the

hydrological regime is dominated by a spring-time snow melt peak. In expGS2a, daily temperatures remain below 0 °C from mid-October until the end of April (Fig. 6c). In May, temperatures rapidly rise towards 10 °C. Consequently, in this example snow accumulated throughout the winter season, after which the snow pack melts in a short period in May, causing a strong runoff peak (Fig. 8b). In expGI1e, however, daily temperatures during winter frequently reach values of a few degrees above 0 °C (Fig. 6b). Thus, in this case part of the snow pack melts during the winter season, making the runoff peak related to the spring snow melt considerably smaller in expGI1e compared to expGS2a (Fig. 8b), despite the higher winter precipitation in the former experiment (Fig. 1b). It can be concluded, therefore, that both the temperature variability during the winter and spring seasons, and the amount of precipitation during GS-2a and GI-1e affect the distribution of runoff events. Consequently, this example shows that changes in atmospheric variability over the GS-2a–GI-1e transition affected fluvial dynamics in northwest Europe.

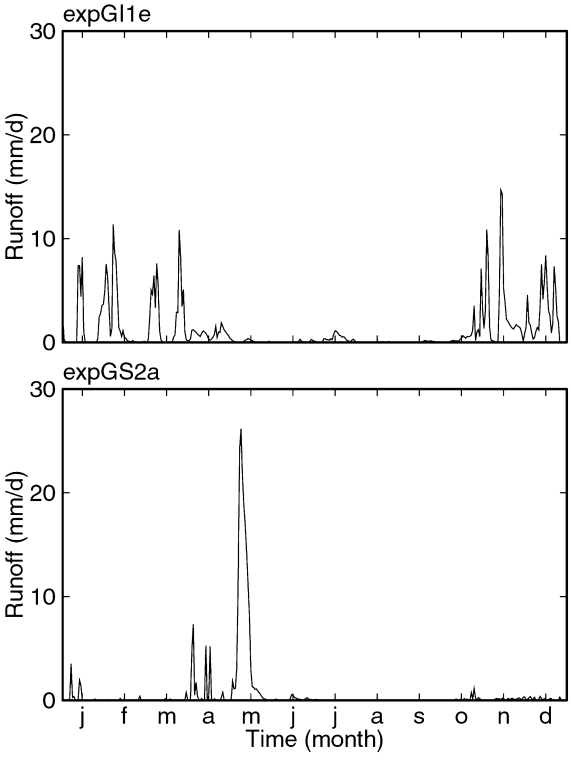

Fig. 8 Surface runoff (mm/d) averaged over five grid cells centred around 52°N, 6°E: **a** expGI1e, **b** expGS2a

5 Concluding remarks

We have presented results of AGCM simulations of the climates during GS-2a and GI-1e to study the change in atmospheric variability over a stadial-interstadial transition, thereby focusing on the North Atlantic region. Our results suggest the following:

1. In the North Atlantic region, the main difference between the GS-2a and GI-1e is found in winter over the central North Atlantic and northwestern Europe. Here, a strong daily variability in temperature is noted for the GS-2a experiment, with regular fluctuations of more than 30 °C within a few days. Moreover, in this experiment also the core of a zone with strong storm activity is located over northwestern Europe. In the experiment for GI-1e, the temperature variability is reduced by about 50%, and the core of the storm track is displaced northwards to the Nordic Seas. Nevertheless, our experiments suggest that daily atmospheric variability during GI-1e was substantially higher than today.
2. The difference between GS-2a and GI-1e can be largely attributed to the northward shift of the sea-ice margin. In the experiment for GS-2a, we prescribed a North Atlantic sea-ice cover down to 48°N, whereas in the GI-1e simulation we assumed an ice-free central North Atlantic and a winter sea-ice cover over the Nordic Seas. As a result, in the GS-2a experiment, a huge reservoir of cold air, cooled below –30 °C over sea-ice was present close to northwest Europe. As Atlantic depressions tend to follow the sea-ice margin (where the steepest temperature gradient is), frequent storms travelled over northwest Europe. These depressions transported cold air (originating over sea-ice) to this region with northerly winds, but also relatively mild air (from the open Atlantic) with southerly winds, thus producing a strong daily temperature variability. In the GI-1e simulation, on the other hand, the sea-ice cover was situated much more to the north, leading to a storm track with a SW–NE orientation, and thus to less frequent storms and smaller temperature fluctuations in northwest Europe.
3. Outside northwest Europe, the change in daily atmospheric variability over the GS-2a–GI-1e transition appears to have been much smaller due to the longer distance to the shift in sea-ice cover.
4. Our inferences suggest that the decrease in daily atmospheric variability over the 14.7 kyr BP transition contributed to a stabilisation of the landscape in Northwestern Europe, for instance through a decrease in the potential for eolian sand transport. This result is consistent with geological and paleoecological data.
5. Our conclusions strongly depend on the prescribed sea surface temperatures and sea-ice margins in the North Atlantic Ocean. Further paleoceanographical studies should confirm these conditions, most notably the extended sea-ice cover prescribed in our GS-2a experiment, which is still under debate (see e.g. discussion in Renssen and Vandenberghe 2002). Moreover, given the uncertainty in ocean surface conditions during the last glacial, it is unclear to what extent our results are valid for other stadial-interstadial transitions.

Acknowledgements The comments of J. Vandenberghe and two anonymous referees are gratefully acknowledged. The Max-Planck-Institut für Meteorologie (in particular L. Bengtsson) and the Deutsches Klimarechenzentrum (in particular M. Lautenschlager)

are thanked for providing computing facilities for the AGCM experiments.

References

Adams JM, Faure H (eds) (1997) Review and atlas of palaeovegetation: preliminary land ecosystem maps of the world since the Last Glacial Maximum. Oak Ridge National Laboratory, TN, USA, at http://www.esd.ornl.gov/projects/qen

Allen PA (1997) Earth surface processes. Blackwell Science, Oxford, pp 404

Atkinson TC, Briffa KR, Coope GR (1987) Seasonal temperatures in Britain during the past 22,000 years, reconstructed using beetle remains. Nature 325: 587–591

Bagnold RA (1941) The physics of wind-blown sands and desert dunes. Methuen, London

Bagnold RA (1973) The physics of blown sands and desert dunes. Chapman and Hall, London, pp 275

Bard E, Arnold M, Maurice P, Duprat J, Moyes J, Duplessy JC (1987) Retreat velocity of the North Atlantic polar front during the last deglaciation determined by ^{14}C accelerator mass spectrometry. Nature 328: 791–794

Bateman MD, van Huissteden J (1999) The timing of last glacial periglacial and aeolian events. J Quat Sci 14: 277–283

Berger AL (1978) Long-term variations of daily insolation and Quaternary climatic changes. J Atmos Sci 35: 2363–2367

Björck S, Walker MJC, Cwynar LC, Johnsen S, Knudsen KL, Lowe JJ, Wohlfarth B, INTIMATE members (1998) An event stratigraphy for the Last Termination in the North Atlantic region based on the Greenland ice-core record: a proposal by the INTIMATE group. J Quat Sci 13: 283–292

Bogaart PW, van Balen RT (2000) Numerical modeling of the response of alluvial rivers to Quaternary climate change. Global Planet Change 27: 147–163

Bohncke SJP (1993) Lateglacial environmental changes in The Netherlands: spatial and temporal patterns. Quat Sci Rev 12: 707–717

Bond G, Broecker W, Johnsen S, McManus J, Labeyrie L, Jouzel J, Bonani G (1993) Correlations between climate records from North Atlantic sediments and Greenland ice. Nature 365: 143–147

Claussen M, Lohmann U, Roeckner E, Schulzweida U (1994) A global data set of land-surface parameters. Max Planck Institute for Meteorology Rep 135, MPI for Meteorology, Hamburg, Germany, pp 30

CLIMAP project members (1981) Seasonal reconstructions of the earth's surface at the Last Glacial Maximum. Geological Society of America Map and Chart Series MC-36, Boulder CO, USA

Coope GR, Lemdahl G, Lowe JJ, Walkling A (1998) Temperature gradients in northern Europe during the last glacial-Holocene transition (14-9 ^{14}C kyr BP) interpreted from coleopteran assemblages. J Quat Sci 13: 419–433

Crowley TJ (1994) Pleistocene temperature changes. Nature 371: 664

Crowley TJ (2000) CLIMAP SSTs re-revisited. Clim Dyn 16: 241–255

DeVernal A, Hillaire-Marcel C, Turon JL, Matthiessen J (2000) Reconstruction of sea-surface temperature, salinity and sea-ice cover in the Northeren North Atlantic during the last glacial maximum based on dinocyst assemblages. Can J Earth 37: 725–750

DKRZ (1994) The ECHAM 3 Atmospheric General Circulation Model. Deutsches Klimarechenzentrum Techn Rep 6, DKRZ, Hamburg, Germany, pp 184

Flückiger J, Dällenbach A, Blunier T, Stauffer B, Stocker TF, Raynaud D, Barnola JM (1999) Variations in Atmospheric N_2O concentration during abrupt climatic changes. Science 285: 227–230

Ganopolski A, Rahmstorf S (2001) Rapid changes of glacial climate simulated in a coupled climate model. Nature 409: 153–158

Guilderson TP, Fairbanks RG, Rubenstone JL (1994) Tropical temperature variations since 20,000 years ago: modulating interhemispheric climate change. Science 263: 663–665

Hoek WZ (1997) Late-glacial and early Holocene climatic events and chronology of vegetation development in The Netherlands. Veget Hist Archaeobot 6: 197–213

Hoskins BJ, Hsu HH, James IN, Masutani M, Sardeshmukh PD, White GH (1989) Diagnostics of the global atmospheric circulation based on ECMWF analyses 1979–1989. World Climate Res Program Techn Rep 27, WCRP, Geneva, Switzerland, pp 217

Hostetler SW, Clark PU, Bartlein PJ, Mix AC, Pisias NJ (1999) Atmospheric transmission of North Atlantic Heinrich events. J Geophys Res 104: 3947–3952

Huisink M (1997) Late-glacial sedimentological and morphological changes in a lowland river in response to climatic change: the Maas, southern Netherlands. J Quat Sci 12: 209–223

Isarin RFB, Renssen H, Koster EA (1997) Surface wind climate during the Younger Dryas in Europe as inferred from aeolian records and model simulations. Palaeogeogr Palaeoclimatol Palaeoecol 134: 127–148

Johnsen SJ, Clausen HB, Dansgaard W, Fuhrer K, Gundestrup N, Hammer CU, Iversen P, Jouzel J, Stauffer B, Steffensen JP (1992) Irregular glacial interstadials recorded in a new Greenland ice core. Nature 359: 311–313

Joussaume S (1993) Paleoclimatic tracers: An investigation using an atmospheric general circulation model under ice age conditions 1. Desert dust. J Geophys Res 98: 2767–2805

Kageyama M, Valdes PJ (2000) Synoptic-scale perturbations in AGCM simulations of the present and Last Glacial Maximum climates. Clim Dyn 16: 517–533

Kageyama M, Valdes PJ, Ramstein G, Hewitt C, Wyputta U (1999a) Northern Hemisphere storm tracks in present day and last glacial maximum climate simulations: a comparison of the European PMIP models. J Clim 12: 742–760

Kageyama M, D'Andrea F, Ramstein G, Valdes PJ, Vautard R (1999b) Weather regimes in past climate atmospheric general circulation model simulations. Clim Dyn 15: 773–793

Kasse C (1997) Cold-climate aeolian sand-sheet formation in north-western Europe (c. 14–12.4 ka); a response to permafrost degradation and increased aridity. Permafrost Periglacial Processes 8: 295–311

Koç N, Jansen E (1994) Response of the high-latitude Northern Hemisphere to orbital climate forcing: evidence from the Nordic Seas. Geology 22: 523–526

Koç N, Jansen E, Haflidason H (1993) Paleoceanographic reconstructions of surface ocean conditions in the Greenland, Iceland and Norwegian Seas through the last 14 ka based on diatoms. Quat Sci Rev 12: 115–140

Koç N, Jansen E, Hald M, Labeyrie L (1996) Late glacial-Holocene sea surface temperatures and gradients between the North Atlantic and the Norwegian Sea: implications for the Nordic heat pump. In: Andrews JT, Austin WEN, Bergsten H, Jennings AE (eds) Late Quarternary Palaeoceanography of the North Atlantic Margins, Geological Society Special Publication vol 111, Geological Society, London, pp 177–185

Leeder MR, Harris T, Kirkby MJ (1998) Sediment supply and climate change: implications for basin stratigraphy. Basin Res 10: 7–18

Lettau K, Lettau H (1977) Experimental and micro-meteorological field studies of dune migration. In: Lettau K, Lettau H (eds) Exploring the world's driest climate. University of Wisconsin, Madison

Lowe JJ, Hoek WZ, INTIMATE group (2001) Inter-regional correlation of palaeoclimatic records for the Last Glacial-Interglacial transition: a protocol for improved precision recommended by the INTIMATE project group. Quat Sci Rev 20: 1175–1187

Mayewski PA, Meeker LD, Whitow S, Twickler MS, Morrison MC, Bloomfield P, Bond GC, Alley RB, Gow AJ, Grootes PM, Meese DA, Ram M, Taylor KC, Wumkes W (1994) Changes in atmospheric circulation and ocean ice cover over the North Atlantic during the last 41,000 years. Science 263: 1747–1751

Mix AC, Bard E, Schneider R (2001) Environmental processes of the ice age: land, oceans, glaciers (EPILOG). Quat Sci Rev 20: 627–657

Peltier WR (1994) Ice age paleotopography. Science 265: 195–201

Raynaud D, Jouzel J, Barnola JM, Chappellaz J, Delmas RJ, Lorius C (1993) The ice record of greenhouse gases. Science 259: 926–933

Renssen H (2001) The climate in The Netherlands during the Younger Dryas and Preboreal: means and extremes obtained with an atmospheric general circulation model. Geol Mijnbouw/Netherl J Geosci 80: 19–30

Renssen H, Isarin RFB (2001) The two major warming phases of the last deglaciation at ~14.7 and ~11.5 kyr cal BP in Europe: climate reconstructions and AGCM experiments. Global Planet Change 30: 117–154

Renssen H, Lautenschlager M (2000) The effect of vegetation in a climate model simulation on the Younger Dryas. Global Planet Change 26: 423–443

Renssen H, Vandenberghe J (2002) Investigation of the relationship between permafrost distribution in NW Europe and extensive winter sea-ice cover in the North Atlantic Ocean during the cold phases of the Last Glaciation. Quat Sci Rev (in press)

Renssen H, Lautenschlager M, Schuurmans CJE (1996) The atmospheric winter circulation during the Younger Dryas stadial in the Atlantic/European sector. Clim Dyn 12: 813–824

Reynolds RW (1988) A real-time global sea surface temperature analysis. J Clim 1: 75–86

Rind D (1987) Components of the ice age circulation. J Geophys Res 92: 4241–4281

Roeckner E, Arpe K, Bengtsson L, Christoph M, Claussen M, Dümenil L, Esch M, Giorgetta M, Schlese U, Schulzweida U (1996) The atmospheric general circulation model ECHAM-4: model description and simulation of present-day climate. Max Planck Institute for Meteorology Rep 218, MPI for Meteorology, Hamburg, Germany, pp 90

Sakai K, Peltier WR (1997) Dansgaard-Oeschger oscillations in a coupled atmosphere-ocean climate model. J Clim 10: 949–970

Sarnthein M, Stattegger K, Dreger D, Erlenkeuser H, Grootes P, Haupt B, Jung S, Kiefer T, Kuhnt W, Pflaumann U, Schäfer-Neth C, Schulz H, Schulz M, Seidov D, Simstich J, van Krefeld S, Vogelsang E, Völker A, Weinelt M (2000) Fundamental modes and abrupt changes in North Atlantic circulation and climate over the last 60 ky – concepts, reconstruction, and numerical modelling. In: Schäfer P, Ritzrau W, Schlüter M, Thiede J (eds) The Northern North Atlantic: a changing environment. Springer, Heidelberg, Berlin New York, pp 45–66

Severinghaus JP, Brook EJ (1999) Abrupt climate change at the end of the last glacial period inferred from trapped air in polar ice. Science 286: 930–934

Taylor KC, Lamorey GW, Doyle GA, Alley RB, Grootes PM, Mayewski PA, White JWC, Barlow LK (1993) The "flickering switch" of late Pleistocene climate change. Nature 361: 432–436

Tucker GB, Barry RG (1984) Climate of the North Atlantic Ocean. In: van Loon H (ed) Climates of the Oceans. World survey of climatology vol 15, Elsevier, Amsterdam, pp 193–257

Valdes PJ, Hall NMJ (1994) Mid-latitude depressions during the last ice-age. In: Duplessy JC, Spyridakis MT (eds) Long-term climatic variations. NATO ASI Series, Vol I 22, Springer, Berlin Heidelberg New York, pp 511–531

Vandenberghe J (1991) Changing conditions of aeolian sand deposition during the last deglaciation period. Z Geomorph N E Suppl Bd 90: 193–207

Vandenberghe J, Nugteren G (2001) Rapid climatic changes recorded in loess successions. Global Planet Change 28: 1–9

van Huissteden J, Schwan JCG, Bateman MD (2001) Environmental conditions and palaeowind directions at the end of the Weichselian Late Pleniglacial recorded in aeolian sediments and geomorphology (Twente, Eastern Netherlands). Geol Mijnbouw/Netherl J Geosci 80: 1–18

Veldkamp A, Tebbens LA (2001) Registration of abrupt climate changes within fluvial systems: insights from numerical modelling experiments. Global Planet Change 28: 129–144